ACS APPLIED MATERIALS & INTERFACES

Article

Pd Nanoparticles Decorated N-Doped Graphene Quantum Dots@N-Doped Carbon Hollow Nanospheres: with High Electrochemical Sensing Performance in Cancer Detection

Jiangbo Xi, Chuyi Xie, Yan Zhang, Lu Wang, Jian Xiao,
Xianming Duan, Jinghua Ren, Fei Xiao, and Shuai Wang

ACS Appl. Mater. Interfaces, **Just Accepted Manuscript** • DOI: 10.1021/acsami.6b05561 • Publication Date (Web): 09 Aug 2016

ACS Publications

ACS Applied Materials & Interfaces is published by the American Chemical Society.
1155 Sixteenth Street N.W., Washington, DC 20036

Pd Nanoparticles Decorated N-Doped Graphene Quantum Dots@N-Doped Carbon Hollow Nanospheres: with High Electrochemical Sensing Performance in Cancer Detection

Jiangbo Xi, [†,‡,§] *Chuyi Xie,* [†,§] *Yan Zhang,* [†,] *Lu Wang,*[†] *Jian Xiao,*[†] *Xianming Duan,*[†] *Jinghua Ren,* [⊥] *Fei Xiao,*[*,†] *and Shuai Wang*[*,†,#]

[†]Key laboratory of Material Chemistry for Energy Conversion and Storage (Huazhong University of Science and Technology), Ministry of Education, School of Chemistry and Chemical Engineering, [#] Flexible Electronics Research Center (FERC), State Key Laboratory of Digital Manufacturing Equipment and Technology, School of Mechanical Science and Engineering, Huazhong University of Science and Technology, Wuhan, 430074, P. R. China.

[‡]School of Chemistry and Environmental Engineering, Wuhan Institute of Technology, Wuhan, 430073, China.

[⊥]Union Hospital, Tongji Medical College, Huazhong University of Science and Technology, Wuhan, 430022, P. R. China.

KEYWORDS Carbon hollow nanospheres, Pd nanoparticles, Graphene quantum dots, Electrocatalyst , Electrochemical biosensor, Cancer detection

ABSTRACT The development of carbon based hollow-structured nanospheres (HNSs) materials has stimulated growing interest due to their controllable structure, high specific surface area, large void space, enhanced mass transport, and good biocompatibility. The incorporation of

functional nanomaterials into their core and/or shell opens new horizons in designing functionalized HNSs for a wider spectrum of promising applications. In this work, we report a new type of functionalized HNSs based on Pd nanoparticles (NPs) decorated double shell structured N-doped graphene quantum dots (NGQDs)@N-doped carbon (NC) HNSs, with ultrafine Pd NPs and "nanozyme" NGQDs as dual signal-amplifying nanoprobes, and explore their promising application as a highly efficient electrocatalyst in electrochemical sensing of a newly emerging biomarker, *i.e.*, hydrogen peroxidase (H_2O_2), for cancer detection. Due to the synergistic effect of the robust and conductive HNS supports and catalytically active Pd NPs and NGQD in facilitating electron transfer, the NGQD@NC@Pd HNS hybrid material exhibits high electrocatalytic activity towards the direct reduction of H_2O_2 and can promote the electrochemical reduction reaction of H_2O_2 at a favorable potential of 0 V, which effectively restrains the redox of most electroactive species in physiological samples and eliminates interference signals. The resultant electrochemical H_2O_2 biosensor based hybrid HNSs materials demonstrates attractive performances, including low detection limit down to nanomole level, short response time within 2 s, as well as high sensitivity, reproducibility, selectivity, and stability, and have been used in real-time tracking a trace amount of H_2O_2 secreted from different living cancer cells in a normal state and treated with chemotherapy and radiotherapy.

1. INTRODUCTION

Cancer diagnosis and therapeutic treatment are of vital importance because of cancer's widespread occurrence, as well as its high death rate and recurrence.[1] Cancer biomarkers are specific molecular probes secreted by tumors or responses of the body to the presence of carcinomas in oncology.[2] Accordingly, the sensitive and reliable detection of cancer biomarkers

provides an effective way for cancer screening and diagnosis, as well as evaluating the pathogenic processes, pharmacological responses to a therapeutic intervention, and prognosis of different cancers.[3] Hydrogen peroxidase (H_2O_2) is the byproduct of many reactions by most oxidases in mitochondria and can generate reactive oxygen species (ROS). The appropriate level of H_2O_2 and ROS plays a critical role in the function and signal transduction of living cells.[4,5] Recently, emerging evidence has demonstrated that several types of tumor cells have generated more H_2O_2 than their normal counterparts due to their :1) higher ROS production; or 2) lower ROS scavenging capacities originated from the abnormal growth of the tumor.[6,7] As a result, the level of H_2O_2 generated from living cancer cells can be utilized as a valuable biomarker of many types of cancer for early stage recognition.

For the clinical detection of H_2O_2, biosensor systems based on electrochemical transducers have attracted tremendous interest due to their prominent advantages, such as high sensitivity and selectivity, rapid response, low cost, user-friendliness, simple instrumentation and the capacity for miniaturization, which make them suitable for *in situ*, real-time and even *in vivo* clinically relevant analytes.[8-11] The electrochemical detection of H_2O_2 is usually based on catalytic reduction of H_2O_2 by a natural enzyme, *e.g.,* horseradish peroxidase (HRP), in an enzymatic electrode system.[12-13] Currently, in parallel with remarkable progress in nanotechnology and electrochemical methods, nanostructured materials have offered exciting opportunities for developing high-performance electrochemical sensors. Nanomaterial-based non-enzymatic artificial sensoring can circumvent the common problems inherent in enzymatic biosensoring attributable to the nature of enzymes. By avoiding such problems, such as high cost, insufficient long-term stability, unsatisfactory reproducibility, and complicated immobilization procedures involved in preparing enzyme electrodes, improved overall sensing

performance can be achieved.[14-15] A diversity of nanomaterials, such as noble metals and metal oxide/sulfide, carbon nanomaterials and their composites with tailorable structures and variable components have been employed in electrochemical non-enzymatic H_2O_2 sensing systems due to their attractive electronic properties, high catalytic activity, low toxicity, and good stability.[16-18] The carbon based hollow structure can enhance the mass diffusion of the substrates and provided electron tunneling to facilitate the electron transfer between the active site and the electrode and led to good electrochemical performance.[19] Furthermore, recent findings have demonstrated that nitrogen-doped carbonaceous materials possess a variety of excellent properties, such as large functional surface area, high ratio of surface active groups to volume, good electrical conductivity and biocompatible C–N microenvironment.[20-22] As a result, the N-doped carbon hollow spheres are anticipated to serve as a good scaffold for loading nanomaterials and improving their catalytic activity. Nevertheless, the efficient reduction or oxidation of H_2O_2 at the surface of nanomaterial-modified electrodes usually requires relatively high over-potential, which leads to the fouling of the electrode and direct faradaic interferences by endogenous electroactive species in biological samples. On the other hand, nanomaterial-based non-enzymatic sensors exhibit intrinsically lower sensitivity than those of enzymatic sensors, and their detection limits towards H_2O_2 usually reach the micromole level. These properties hinder their practical application in highly sensitive and selective detection of H_2O_2 clinical sample analysis.

In this work, we present the design and fabrication of a new type of electrocatalyst based on Pd nanoparticles (NPs) decorated double shell structured N-doped graphene quantum dots@N-doped carbon (NC) hollow nanospheres (HNSs), and explore their clinical application in electrochemical non-enzymatic H_2O_2 sensing system for ultra-sensitive and highly specific

detection of extracellular H_2O_2 molecules released from living cancer cells. Pd NPs have been well-developed as highly efficient noble metal nanocatalysts in non-enzymatic electrochemical H_2O_2 sensoring due to their high electrocatalytical activity towards reduction and/or oxidation of H_2O_2.[23, 24] Meanwhile, graphene quantum dots (GQD), the nanometer-sized fragments of graphene, have exhibited unique optical and electronic properties due to their quantum confinement and edge effects.[25] Most recently, GQD has been found to possess intrinsic peroxidase mimetic activity, and could function as a biomimetic HRP in the nanomaterial-based artificial enzymes, *i.e.,* a "nanozymes" biosensing system.[26, 27] Herein, ultrafine Pd NPs with average size of 2.9 nm and nitrogen-doped GQD (NGQD) are incorporated into NC-HCSs architecture to form an NGQD@NC@Pd HNS hybrid material and act as dual signal-amplifying nanoprobes in a H_2O_2 sensing system. NC-HNS materials possess superior physical and chemical properties, including high surface-area-to-volume ratio, large void space, enhanced masstransport, controllable structure and robust chemical inertness,[28, 29] which can serve as a robust and electronically conductive catalyst support to reduce ohmic resistance, facilitate the high loading and well dispersion of Pd NPs and NGQD on its surface, and enhance their catalytic activity and stability. Owing to the synergistic effect from the structural and compositional merits of catalytically active species and the HNS supports, the NGQD@NC@Pd HNS hybrid material exhibited a large surface area, fast electron transfer rate, and high electrocatalytic activity towards the direct redox of H_2O_2. When implemented in the electrochemical detection of H_2O_2, the resultant nanomaterial-based non-enzymatic sensor showed good performance, including a wide linear detection range up to 1.4 mM, low detection limit of 20 nM, high sensitivity of 0.59 mA mM^{-1} cm^{-2}, favorable operating potential of 0 V, as well as good reproducibility, stability, and anti-interference ability. Moreover, it could be used in ultra-

sensitive and specific detection of a trace amount of H_2O_2 released from different living tumor cells in a normal state or under chemotherapy and radiotherapy.

2. MATERIALS AND METHODS

2.1. Materials. All solutions were prepared using deionized water (resistivity > 18 Ω cm^{-1}). N-formyl-methionyl-leucyl-phenylalanine (fMLP), 3-aminopropyltrimethoxysilane (97%) and SiO_2 spheres with sizes ranging from 350 to 400 nm, and were purchased from Sigma-Aldrich. Dopamine hydrochloride (98%) and tris (hydroxymethy1) aminomethane (Tris, 99.8%) were purchased from Aladdin Chemistry Co., Ltd., China. K_2PdCl_4 (99%) was purchased from Sinopharm Chemical Reagent Co. (China). Dulbecco's modified eagle's medium (DMEM), fetal bovine serum (FBS), trypsine-EDTA (0.25%), and penicillinstreptomycin were purchased from HyCl one (Waltham, MA, USA). The human living cells MDA-MB-231, HBL-100, and U87 were obtained from the American Type Culture Collection (ATCC, Manassas, VA, USA). The cells were cultured at 37°C, 5% CO_2 in DMEM supplemented with 10% FBS, 100 IU mL^{-1} penicillin and 100 mg mL^{-1} streptomycin. The chemotherapeutic agent cisplatin (DDP) was purchased from Sigma (USA).

2.2. Synthesis of af-SiO_2@GQDs spheres. GQDs were prepared according to a bottom-up method.[25] For the synthesis of af-SiO_2 nanospheres, 200 mg of SiO_2 spheres were firstly dispersed in 100 mL ethanol by sonication for 30 min. Then 1 mL of 3-aminopropyltrimethoxysilane was added and the mixture was stirred for 5 h. The products were then centrifugated and rinsed with ethanol. For the synthesis of af-SiO_2@GQDs nanospheres, 250 mL of 1 mg mL^{-1} GQDs aqueous solution was added into the af-SiO_2 nanospheres

suspension and the mixture was stirred for 1 h. Finally, the products were collected by centrifugation, washed with water for several times, and then dried at 60°C overnight.

2.3. Synthesis of af-SiO_2@GQDs@PDA nanosphere. 150 mg of as-prepared af-SiO_2@GQDs spheres were dispersed in 50 mL of 3 $mgmL^{-1}$ dopamine Tris solution (pH 8.5, 10 mM Tris buffer) and allowed to proceed for 36 h under stirring at room temperature. The resultant af-SiO_2@GQDs@PDA was separated and collected, and subsequently washed for 5 cycles and dried by freeze drying.

2.4. Synthesis of NGQDs@NC@Pd HNS. 200 mg of af-SiO_2@GQDs@PDA were dispersed in 50 mL of DI water. Then 50 mg of K_2PdCl_4 was added, and the mixture was kept in a vial under vigorous stirring for 30 min in an ice bath. After the reaction, the Pd NPs decorated af-SiO_2@GQDs@PDA (af-SiO_2@GQDs@PDA@Pd) nanospheres was obtained, which was separated from the suspension and subsequently washed with ultrapure water for 5 times and dried by freeze drying. The SiO_2@NGQDs@NC@Pd nanospheres were prepared by carbonizing af-SiO_2@GQD@PDA@Pd nanospheres at 500 °C for 3 h under inert atmosphere. Finally, the af-SiO_2 cores were etched by HF solution (~2%), and the NGQDs@NC@Pd HNSs were obtained. For comparison, NC@Pd and NGQDs@NC HNSs were also fabricated under the same conditions and used as control samples.

2.5. Preparation of different modified electrodes. The as-obtained NGQDs@NC@Pd HNSs powdery sample was dispersed in deionized water, with ultrasonic agitation to give 1.0 mg mL^{-1} suspension. 10 μL of the suspension was dropped on a cleaned glass carbon electrode (GCE) and the solvent was evaporated in air. A uniform film coated electrode (NGQDs@NC@Pd/GCE) was obtained. The NC@Pd/GCE and NGQDs@NC/GCE were fabricated under the same procedure. Before the electrochemical measurement,

NGQD@NC@Pd/GCE had been activated by CV scanning for 20 cycles in the potential range of -0.6 to +0.6 V (versus Ag/AgCl electrode).

3. RESULTS AND DISCUSSION

The preparation process of the proposed NGQD@NC@Pd HNS has been schematically illustrated in Figure 1. SiO_2 nanospheres were firstly modified by 3-aminopropyltrimethoxysilane to introduce amine groups on their surface (step 1 in Figure 1). GQD nanosheets prepared by a bottom-up method [25] were utilized to wrap the amino-functionalized SiO_2 (af-SiO_2) nanospheres through electrostatic interaction and hydrogen bonds between the amino group on af-SiO_2 and the oxygen-containing groups on GQD (step 2 in Figure 1).[30] The af-SiO_2@GQD nanospheres were further coated by a layer of polydopamine (PDA) *via* self-polymerization of dopamine (DA) hydrochloride on their surface (step 3 in Figure 1).[31] Pd NPs were then *in situ* grown on the surface of af-SiO_2@GQD@PDA nanospheres using K_2PdCl_4 as the precursor, in which the PDA layer served as both the reducing and capping agent (step 4 in Figure 1).[23] As demonstrated in step 5 of Figure 1, the as-prepared Pd NPs decorated af-SiO_2@GQD@PDA (af-SiO_2@GQD@PDA@Pd) nanospheres were converted to af-SiO_2@NGQD@NC@Pd nanospheres by carbonizing at 500 ^oC for 3 h under inert atmosphere. After etching the SiO_2 cores with HF solution, the NGQD@NC@Pd HNSs have been obtained.

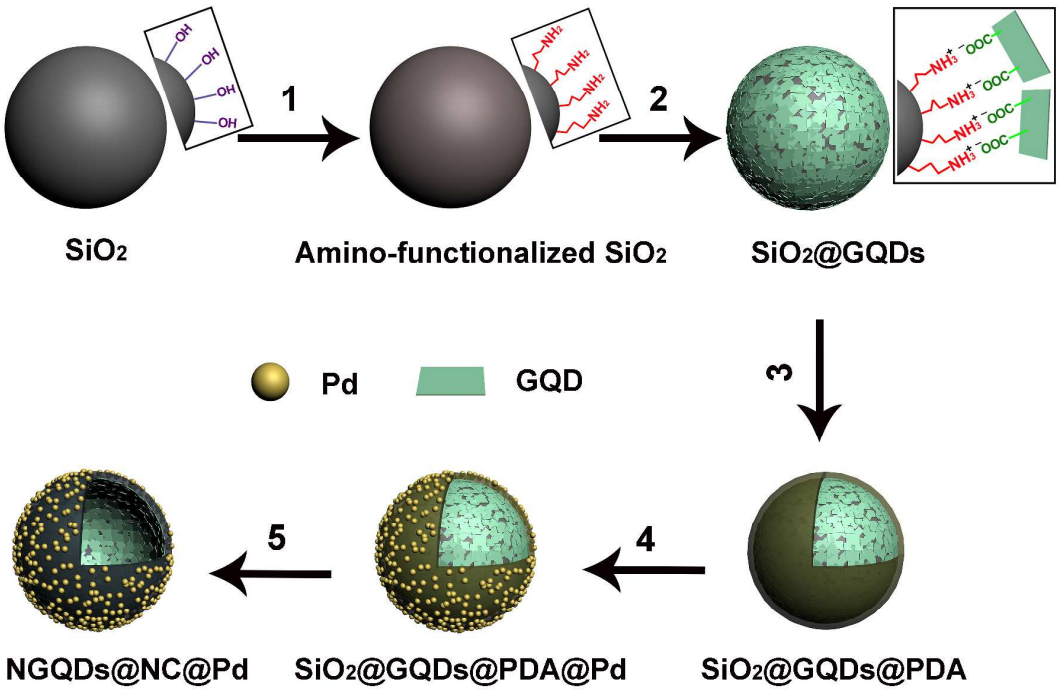

Figure 1 Schematics illustrating the preparation process of NGQDs@NC@Pd HNSs. (1) Amino-functionalization of SiO_2 nanospheres; (2) Wrapping SiO_2 nanospheres with GQD nanosheets; (3) Coating of PDA on surface of SiO_2@GQD; (4) Loading of Pd NPs on the surface of SiO_2@GQD@PDA; (5) Further carbonization and HF etching to form NGQD@NC@Pd HNSs.

The morphologies of the nanomaterials obtained by different steps have been shown in Figure 2. GQDs were prepared according to a bottom-up method.[25] The atomic force microscopy (AFM) result indicates that the GQDs (Figure 2A) are mostly nanosheets of ~ 15 nm in size, whose height is mostly distributed in the range of 0.5~3.0 nm. In addition, the GQDs suspension gives a blue light emission under the excitation by 365 nm UV light (Inset of Figure 2A). The amino-functionalized SiO_2 (af-SiO_2) nanospheres SiO_2 nanospheres (350~400 nm in diameter, Figure 2B) were wrapped by GQDs to form af-SiO_2@GQD nanospheres (Figure 2C). During this procedure, the color of the SiO_2 nanospheres changes from their original white to yellow

brown (inset of Figure 2B and 2C). The af-SiO_2@GQD nanospheres were further coated by a layer of PDA (Figure 2D), upon which the color changes from yellow brown to dark brown (inset of Figure 2D). Pd NPs were then *in situ* grown on the surface of af-SiO_2@GQD@PDA nanospheres using K_2PdCl_4 as the precursor to form af-SiO_2@GQDs@PDA@Pd nanospheres (Figure 2E). After carbonizing and etching the SiO_2 cores with HF solution, the NGQD@NC@Pd HNSs have been obtained (Figure 2F), which exhibit a highly integrated structure in their high-magnification scanning electron microscope (SEM) image (Figure 2G) and a very uniform size in their low-magnification SEM image (Supporting Information, Figure S1).

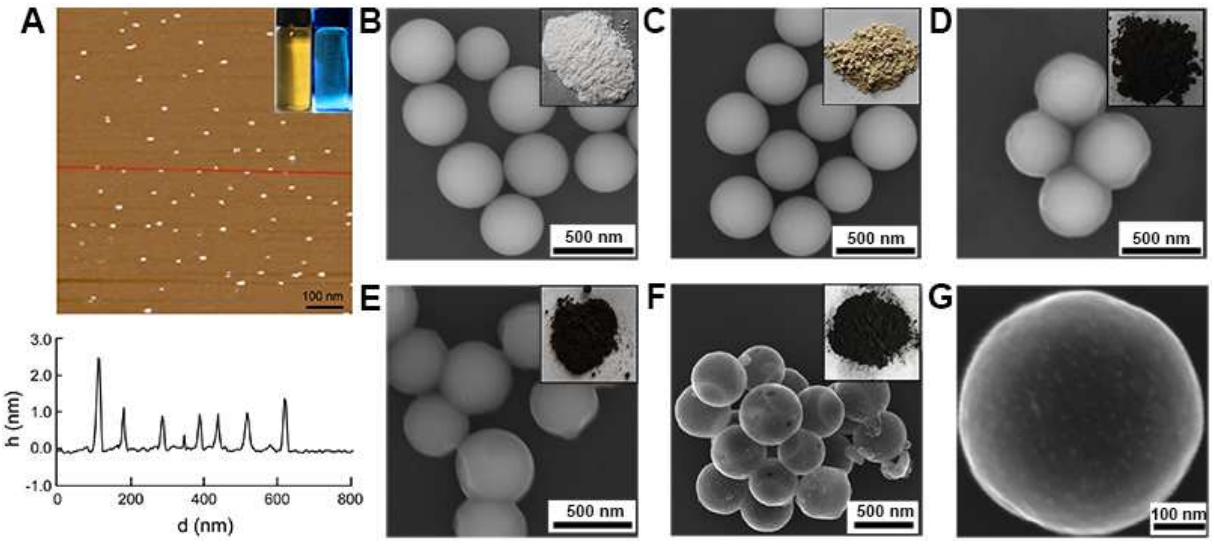

Figure 2 (A) AFM image of GQDs, the inset shows photographs of the GQDs suspension taken under visible light (left) and under 365 nm UV light (right). SEM images of (B) af-SiO_2 nanospheres; (C) af-SiO_2@GQDs nanospheres; (D) af-SiO_2@GQDs@PDA nanospheres; (E) af-SiO_2@GQDs@PDA@Pd nanospheres; (F) and (G) NGQDs@NC@Pd HNS with different magnification. Insets are their corresponding photographs.

Figure 3A-3C displays the typical transmission electron microscope (TEM) image of the NGQD@NC@Pd HNS, in which highly dense Pd NPs are anchored on the surface of NGQD@NC@Pd HNSs. Furthermore, the interplanar spacings for the lattice fringes of Pd NPs on the NC layer are 0.223 nm and 0.195 nm, which correspond to the (111) and (200) lattice planes of the face-centered cubic (fcc) Pd structure, respectively (Figure 3D).[32] The corresponding dark-field scanning transmission electron microscope (DF-STEM) images of NGQD@NC@Pd HNSs are shown in Figures 3E and 3F, which visualize the high loading and thorough dispersion of Pd NPs throughout the entire NGQD@NC HNSs. From the high-resolution DF-STEM image shown in the Figure 3G, it can be discriminated by contrast ratio that the NGQD layer and NC layer exhibit thicknesses of ~10 nm and ~ 30 nm, respectively. The majority of Pd NPs are ultrafine with a mean size of 2.9 nm (Figure 3H), and only few sintered NPs show larger particle size even after the annealing treatment. These results demonstrate an excellent thermal stability of NGQD@NC@Pd catalyst. The element distribution shown in energy dispersion spectroscopy (EDS) elemental mappings from the high-magnification TEM image (Figure 3I), further verifies the homogeneous distribution of different elements, including C, O and N, as well as the uniform dispersion of Pd NPs on NGQD@NC HNSs.

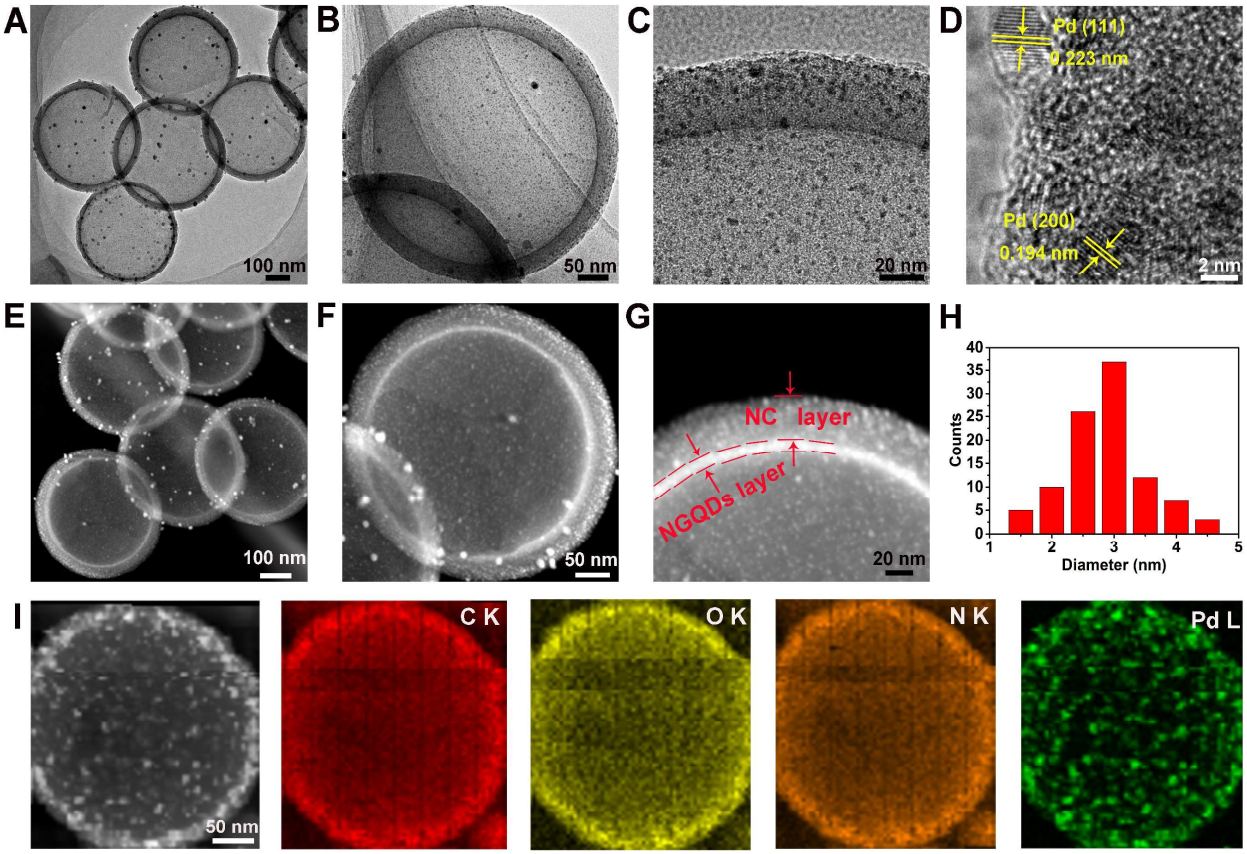

Figure 3 (A)-(D) TEM images and (E)-(G) DF-STEM images of NGQDs@NC@Pd HNSs with different magnifications. (H) Statistic histogram of Pd particles size distribution on NGQDs@NC@Pd HNS. For the particle-size distribution determination, *ca.* 100 NPs were counted at several identical locations. (I) HRTEM image of NGQDs@NC@Pd HNS and its corresponding EDS elemental mappings.

The surface composition of NGQD@NC@Pd HNSs has been further characterized by X-ray photoelectron spectroscopy (XPS) and microwave plasma-atom emission spectrometer (MP-AES). The XPS survey spectrum reveals the presence of C, N, O and Pd signals in the sample (Figure S3), which is consistent with the element composition of NGQD@NC@Pd HNSs shown in Figure 3E. The high-resolution spectrum of C 1s can be deconvoluted into four single peaks

(Figure 4A), these peaks correspond to C-C or C=C (284.6 eV), C-N (285.3 eV), C=N (286.5 eV) and quinone C=O (288.3 eV), originating from the NGQD layer and the NC layer in NGQD@NC@Pd HNS.[33, 34] In the O1s spectrum (Figure 4B), the peaks located at the binding energies of 531.1 eV, 532.1 eV and 533.3 eV are assigned to C=O, COOH and C-O, respectively.[33] The peak at 532.1 eV can be attributed to COOH originating from the GQD layer.[25] The N 1s spectrum reveals the presence of several nitrogen-containing groups, including pyridinic N/C=N (398.5 eV), amine (399.5 eV), pyrrolic N/C-NH (400.4 eV),[33] and graphitic N (401.4 eV)[35] (Figure 4C). The N 1s spectrum of the NGQD@NC@Pd HNS sample exhibits an extra signal from graphitic N in comparison to that of the NC@Pd HNS sample (Figure S4), further confirming that N heteroatoms have been doped into the GQD framework and NGQD was obtained. The atomic concentration of nitrogen is 5.89%. The Pd 3d spectrum, shown in Figure 4D, demonstrates that two spin-orbital doublets accounted for two electronic states of Pd, *i.e.*, Pd (0) and Pd (II), respectively.[36] The distinct peaks at 335.9 eV and 341.3 eV are assigned to Pd (0), and the weak peaks at 338.3 eV and 343.2 eV indicate the presence of Pd(II) due to the partially oxided Pd in the NGQD@NC@Pd HNS sample. The Pd content in the NGQD@NC@Pd HNS composite was determined using MP-AES, which was measured to be as low as 3.45 wt.%.

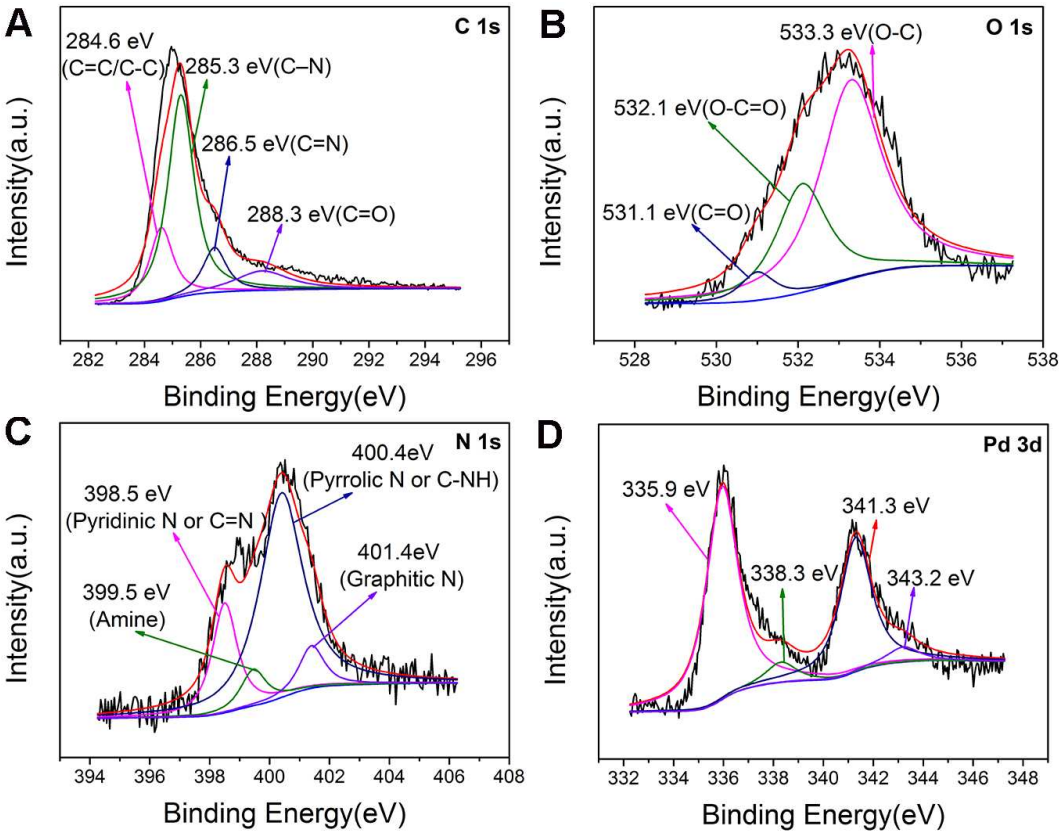

Figure 4 XPS spectra of (A) C 1s, (B) O 1s, (C) N 1s and (D) Pd 3d in NGQDs@NC@Pd HNSs.

The electrochemical properties of NGQD@NC@Pd, as well as NGQD@NC and NC HNSs, have been explored by modifying them on a glass carbon electrode (GCE, 3 mm in diameter, Figure S5). $Fe(CN)_6^{3-/4-}$ was firstly employed as a redox probe to investigated the cyclic voltammetry (CV) behaviors of different modified GCE (Figure S6). The CV curve of pristine NC HNSs modified GCE (NC/GCE) exhibits an ideal peak potential separation (ΔE_p) value of approximately 59 mV, indicating that the highly conductive NC HNSs have facilitated the heterogeneous electron transfer between the electrode and the $[Fe(CN)_6]^{3-/4-}$ redox species. However, owing to the blocking effect of electron transfer originating from the electrostatic repulsion between negative NGQD species and the $Fe(CN)_6^{3-/4-}$ probe, the ΔE_p value increases to 75 mV for NGQD@NC HNSs modified GCE (NGQD@NC/GCE). Furthermore, the

ΔE_p value for NGQD@NC@Pd HNSs modified GCE (NGQD@NC@Pd/GCE) decreases to 64 mV due to the decoration of numerous ultrafine Pd NPs on NGQD@NC HNSs (Figure S6), which provide the necessary conduction pathways and improve electron transport properties. The electroactive surface area (ESA) of different electrodes are estimated according to the Randles–Sevcik equation[37] to be 0.57, 0.36, 0.23 and 0.07 cm^2 for NGQD@NC@Pd/GCE, NGQD@NC/GCE, NC/GCE and bare GCE, respectively. Benefitting from the large specific surface area of NCHNSs, and high-loading and thoroughly dispersed NGQD and Pd NPs on their inner and outer surfaces, the resultant NGQD@NC@Pd/GCE exhibits the largest ESA value, which is more than eight times greater than that of bare GCE.

Figure 5A presents the cyclic voltammetry (CV) curves for all of the modified electrodes in a 0.1 M phosphate buffer solution (PBS, pH 7.4) containing 1.0 mM H_2O_2. The NC/GCE exhibits negligible electrocatalytic activity towards the redox reactions of H_2O_2, and there are also no distinct reduction or oxidation peaks on NC/GCE over a wide voltage range from -0.6 to 0.6 V. Meanwhile, for both NGQD@NC/GCE and NC@Pd/GCE, an obvious reduction peak of H_2O_2 was observed at -0.45 V and -0.09 V, respectively, and the peak currents increased linearly with the higher H_2O_2 concentration in PBS (Figure S7A and 7B). Evidently, NGQD@NC@Pd nanohybrid material demonstrates an enhanced electrocatalytic activity towards H_2O_2 reduction. When the reduction peak of H_2O_2 on NGQDs@NC@Pd/GCE shifts to -0.04 V, the peak current density increases more than 2 times than that on NGQDs@NC/GCE at -0.45 V, and is also 1.5 times larger than that on NC@Pd/GCE at -0.09 V. The dramatically enhanced electrocatalytic activity of NGQD@NC@Pd nanocomposite arises from the synergistic contribution of the inner NGQD and outer Pd NPs on dual functionalized NGQD@NC@Pd HNSs. As demonstrated previously, the GQD possesses unexpected peroxidase mimetic activity, and can be used as

nanozymes to substitute for natural peroxidase enzymes in biotechnology and bioengineering.[26, 27] Meanwhile, Pd NPs have been recognized as highly efficient noble metal electrocatalysts towards the reduction and/or oxidation reaction of H_2O_2, and their electrocatalytical activities highly dependent on their size and distribution. The NC HNS scaffold enables the high loading and thorough distribution of NGQD and Pd NPs upon it, which in turn provides more reaction active sites for the electrocatalytic reduction of H_2O_2.

The CV curves of NGQD@NC@Pd/GCE in PBS containing H_2O_2 at various concentrations (*i.e.*, 0, 1, 2, 3, 4 and 5 mM) are presented in Figure 5B. The reduction peak potentials of H_2O_2 shift negatively, and the peak current densities increase linearly with each incremental increase of the H_2O_2 concentration in PBS. The linear range, detection limit, and sensitivity of electrochemical H_2O_2 sensor based on NGQD@NC@Pd/GCE have been determined by amperometric measurement at the optimal potential of 0 V. With successive step increases of H_2O_2 concentration in PBS, a well-defined, steady-state amperometric current variation was triggered within 2s (Figure 5A and inset a), indicating the stable and efficient electrocatalytic property of NGQD@NC@Pd nanocomposite on the electrode. The calibration plots of the amperometric current as a function of H_2O_2 concentration are shown in the Figure 5C inset b, which exhibits an expanded linear response range up to 1.4 mM (R^2=0.999), with a sensitivity of 0.59 mA cm^{-2} mM^{-1} and a low detection limit of 20 nM based on a signal-to-noise ratio of 3:1 (Figure 5C inset c). These findings are superior to other non-enzymatic H_2O_2 sensors reported in the literature published over the past year (Table S1),[7, 23, 38-46] thus demonstrating improved sensing performance for the highly sensitive detection of H_2O_2 by NGQD@NC@Pd/GCE.

Other performance parameters of GQD@NC@Pd/GCE with respect to reproducibility, selectivity and stability are crucial for *in vivo* and *in vitro* H_2O_2 detection, and therefore have

been explored in detail using amperometric measurement. The current response for eight replicates of 20 μM H_2O_2 solution on one NGQD@NC@Pd/GCE yielded a relative standard deviation (RSD) value of 2.7 %, and reproducible current responses with RSD value less than 3.6% were detected for eight different NGQD@NC@Pd/GCE in 20 μM H_2O_2 (Figure S8), indicative of the good repeatability and reproducibility of GQD@NC@Pd/GCE. The selectivity of GQD@NC@Pd/GCE has been investigated by injecting the analyte and some possible electroactive interfering reagents in blank PBS and monitoring their amperometric current response. The responses were observed in the initial solution and then with the addition of 20 and 50 μM H_2O_2, respectively. No detectable amperometric responses were observed when adding certain amounts (*i.e.,* 20 and 50 μM) of several electroactive compounds, *i.e.,* cathodic interference oxygen (O_2) and anodic interferences DA, ascorbic acid (AA) and uric acid (UA), in PBS containing equal amount of H_2O_2. The good selectivity is benefit from the favorable applied potential of 0 V for the amperometric detection of H_2O_2, which effectively restrains the redox of most electroactive species in physiological samples and eliminates interference signals (Table S2). Long-term stability and cycling stability have been examined by measuring a glucose solution intermittently and successively. The NGQD@NC@Pd/GCE maintains over 90% of its initial current response to 0.1 mM H_2O_2 after being stored in air at room temperature for 30 days or over 50 successive tests of one NGQD@NC@Pd/GCE. These results indicate the good stability of NGQD@NC@Pd nanocomposite, originating from its unique HNS structure in immobilizing electrocatalytically active nanomaterials.

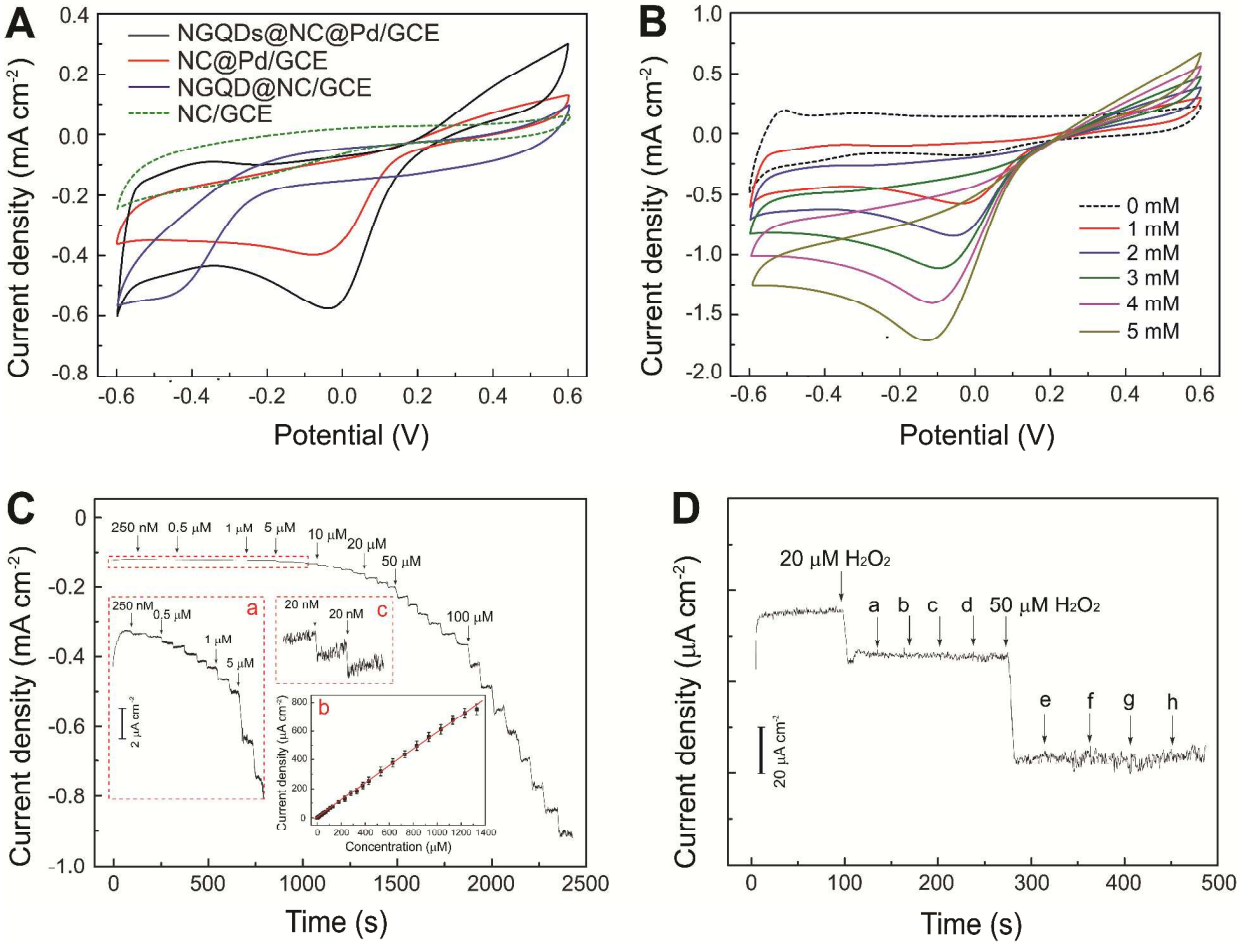

Figure 5 (A) CV curves of NGQDs@NC@Pd/GCE, NC@Pd/GCE, NGQDs@NC/GCE and NC/GCE in PBS (pH 7.4) containing 1.0 mM H_2O_2. Scan rate: 50 mV s^{-1}. (B) CV curves of NGQDs@NC@Pd/GCE in PBS (pH 7.4) containing 0, 1, 2, 3, 4 and 5 mM H_2O_2 (from top to bottom). Scan rate: 50 mV s^{-1}. (C) Amperometric response of NGQDs@NC@Pd/GCE with successive step changes of H_2O_2 concentration. The insets are the enlarged graph of the highlight region of Figure C (a), the corresponding calibration curves (b), and the amperometric response of NGQDs@NC@Pd/GCE with successive step changes of 20 nM H_2O_2 (c). (D) Influence of 20 μM O_2 (a), DA (b), UA (c), AA (d) and 50 μM O_2 (e), DA (f), UA (g), AA (h) on the amperometric response of equal amount of H_2O_2 in 0.1 M PBS (pH 7.4). Applied potential: 0 V.

The practical application of the as-prepared electrochemical non-enzymatic sensor based on NGQD@NC@Pd/GCE has been explored for detecting cancer biomarkers and assessing the therapeutic effect of cancer, as well. Worldwide, breast cancer accounts for 25% of total cancer cases and has become the leading cause of cancer mortality among females.[47, 48] Nonetheless, breast cancer has the best prognosis when diagnosed at early stages, and the development of effective methods for early detection is of great significance to improve the overall survival rate. MDA-MB-231, MCF-7 and T47D are three types of human breast cancer cell lines, and account for over two-thirds of all abstracts reporting studies on the aforementioned breast cancer cell lines, as concluded by a Medline-based survey.[49] Therefore, MDA-MB-231 was chosen here as the model to investigate the electrochemical sensing performances of NGQD@NC@Pd/GCE towards living tumor cell lines, using non-tumorigenic human breast cell lines, *i.e.,* HBL-100 human breast epithelial cells as the control. Before electrochemical experiments, the microscopy technology and standard cell counting Kit-8 (CCK-8) assay were employed to evaluate the cytotoxicity of the NGQD@NC@Pd/GCE. As shown in the bright-field and dark-field fluorescent images of Figures 6A and 6B, respectively, MDA-MB-231 and HBL-100 cells remain healthy when incubated with NGQD@NC@Pd/GCE for over 4 h. The results of the CCK-8 assay demonstrate that both of these two cells maintain over 95% viability after 4 h incubation with the NGQD@NC@Pd/GCE (Figure 6C), indicative of the good biocompatibility of the NGQD@NC@Pd/GCE. The electrochemical testing of H_2O_2 released from different living cells was performed by a three-electrode system in 6-well plates containing living cells with 80% confluency, using NGQD@NC@Pd/GCE as the working electrodes. N-Formylmethionyl-leucyl-phenylalanine (fMLP), a potent polymorphonuclear leucocyte chemotactic factor, has been utilized as an artificial stimulator to irritate living cells to release ROS by disrupting intracellular

redox homeostasis.[50,51] As shown in Figure 6D, upon the addition of 0.1 mM fMLP in each tested well, significantly increased amperometric current densities of 0.54 μA cm^{-2} and 0.44 μA cm^{-2} were obtained in the presence of MDA-MB-231 and HBL-100, respectively. After adding 500 U/mL catalase, a selective scavenger of H_2O_2, the amperometric current responses gradually declined to a background level due to the decomposition of H_2O_2 by catalase. By comparison, upon the addition of equal amounts of fMLP or catalase, no measurable signals were observed in control tested wells without living cells. These results constitute proof that the increased amperometric currents are attributable to the electrochemical reduction of H_2O_2 secreted from living cells upon the stimulation by fMLP. As demonstrated in previous work, when living cells are stimulated by external elements, they will excrete more H_2O_2 induced by oxidative stress reaction, and their intracellular redox homeostasis will be disrupted.[4, 5] In order to maintain the redox homeostasis state, the excess H_2O_2 will diffuse out across the lipid bilayer or aquaporins of membrane to keep the intracellular H_2O_2 concentration at the normal level.[52, 53] The extracellular H_2O_2 converts from molecular-recognition events into measurable outputs by electrochemical transducers based on the proposed electrode. Noticeably, tumor cell line MDA-MB-231 secreted more H_2O_2 than normal cell line HBL-100 upon being stimulated. As mentioned above, many types of tumor cells generate more H_2O_2 than their normal counterparts upon being stimulated. In this work, H_2O_2 has been demonstrated to be an effective biomarker to identify the tumor cell line and its normal counterparts.

The effect of cancer chemotherapy has also been assessed by the proposed electrochemical methods based on NGQD@NC@Pd/GCE. In this work, the living cancer cell line MDA-MB-231 has been treated with cisplatin (DDP), a chemotherapeutic agent that is widely used in clinic to resist several types of tumors. The results show that, upon the addition of 0.1 mM fMLP in

tested wells containing MDA-MB-231 cells treated with DDP, the increment of amperometric current densities was 0.45 μA cm^{-2}, representing an 18.2% decrease in the absence of any treatment (Figure 6F). As manifested by a plethora of experiments that cis-platinum complex is an ultimate cytotoxic agent of administered antitumor drug.[54, 55] It possesses high therapeutic activity against tumors by strongly interacting with nucleobase N-donors of DNA molecule to perturb the tumor structure and inhibit DNA replication, which results in cancer cell death.[56,57] Therefore, undergoing chemotherapy by DDP results in killing living cancer cells and releasing less H_2O_2 upon being simulated. The cytotoxicity of DDP towards MDA-MB-231 cells has also been evaluated by CCK-8 assay. The results indicate that, under treatment with DDP, cell viability decreased by 17%, which is consistent with that obtained by electrochemical amperometric tests based on NGQD@NC@Pd/GCE.

Furthermore, the radiotherapy effect of cancer cells has been investigated using U87 cell lines as the models. In cell biology, U87 is a human primary glioblastoma cell line and exhibits epithelial morphology,[58] as shown in Figures 6G and 6H. U87 glioma cells have been shown to contribute to the brain tumor stroma. Patients suffering from it usually have a worsened prognosis and higher risk of relapse.[59] Radiotherapy has been considered an effective therapeutic approach against brain tumors.[60] Electrochemical experiments were performed to evaluate the sensing performance of NGQD@NC@Pd/GCE towards H_2O_2 released from U87 under radiotherapy. Firstly, the CCK assay showed that U87 cells maintain over 95% viability after 4 h incubation with NGQD@NC@Pd/GCE (Figure 6I), indicating the low cytotoxicity of NGQD@NC@Pd/GCE. Electrochemical experiments show that, upon being stimulated by fMLP, an increased amperometric current density of 0.30 μA cm^{-2} has been observed on NGQD@NC@Pd/GCE in tested wells containing U87 cells (Figure 6J). After two hours from

the radiotherapy treatment, the value decreases to 0.26 A cm^{-2}, which is 86.7% of that without treatment. And after four hours from the radiotherapy treatment, the values decrease to 0.17 μA cm^{-2}, which is 56.7% of that without treatment (Figure 6K and 6L). As demonstrated, exposing living cells to radiation treatments will lead to an imbalance between oxidants and antioxidants, and increase the accumulation of ROS. The excessive production of ROS then increases the ROS stress to a point that triggers cell death.[61, 62] Therefore, many living cancer cells die in the period following radiation exposure, causing a decreased amount of H_2O_2 to be secreted from living cells, and the corresponding amperometric current densities decrease accordingly. All of these results demonstrate that the proposed electrochemical measurement of extracellular H_2O_2 under varying conditions using GQD@NC@Pd/GCE provides a highly effective and accurate method to evaluate the living cell oxidative stress capability, as well as distinguish different living cells and explore their microenvironment. These findings could be potentially useful for the pathological diagnosis of cancer, as well as evaluating the pharmacokinetics and therapeutic efficacy in the treatment of cancer.

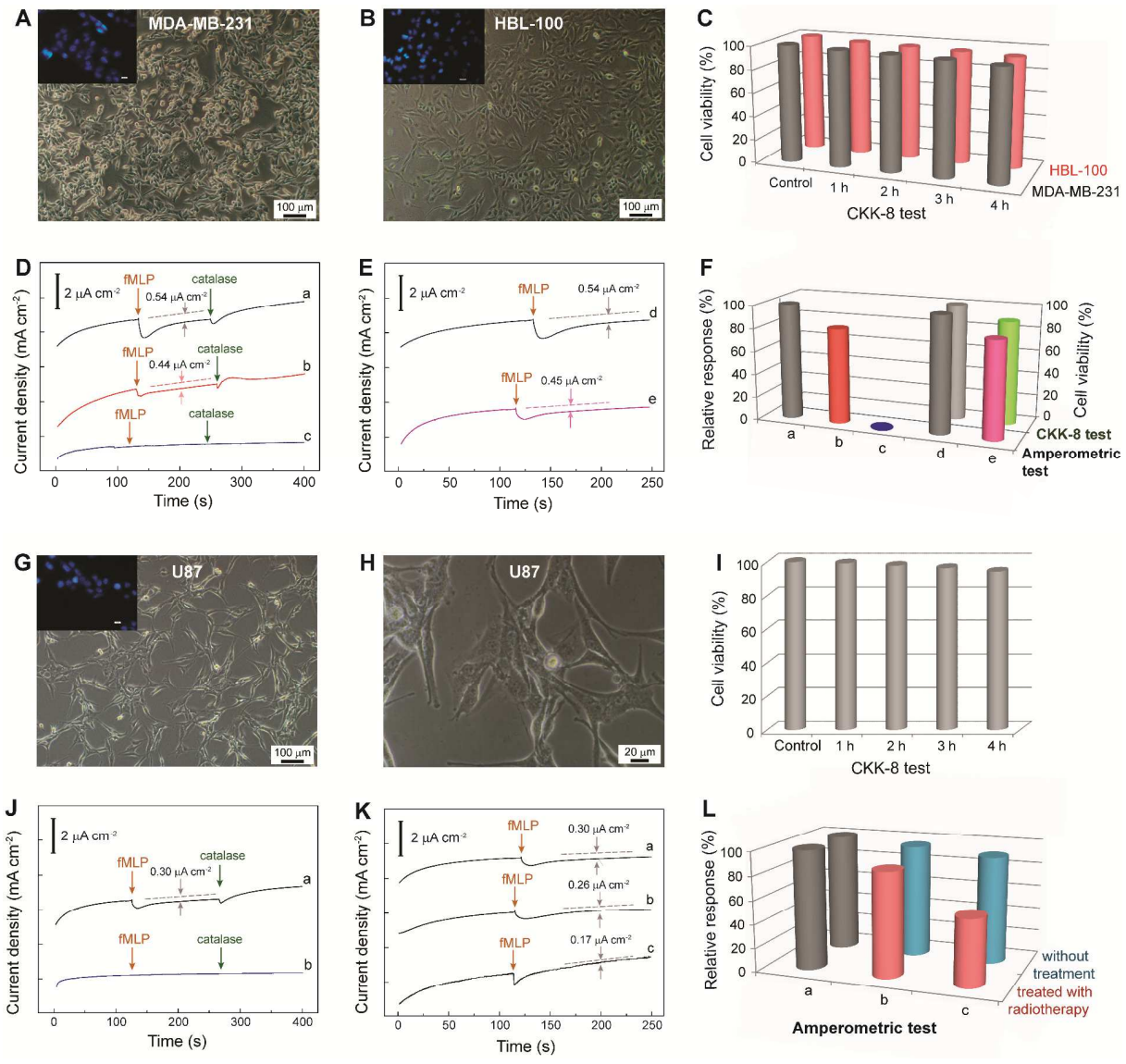

Figure 6 (A) and (B) Bright-field and dark-filed microscope images of various living cells after being incubated with NGQDs@NC@Pd/GCE. (C) Quantitative cell viability results of CCK-8 assay. (D) Amperometric responses of NGQD@NC@Pd/GCE to the addition of 0.1 mM fMLP and 500 U/mL catalase in tested well with MDA-MB-231 cells (a), HBL-100 cells (b) and without cells (c). (E) Amperometric responses of NGQDs@NC@Pd/GCE to the addition of 0.1 mM fMLP in tested well containing MDA-MB-231 cells without treatment (d) and treated with DDP (e). (F) Corresponding histograms of the amperometric responses of (D) and (E), and the results of CCK-8 assay of the cytotoxicity of DDP towards MDA-MB-231 cells. (G) and (H)

Bright-field and dark-filed microscope images of U87 cells after being incubated with NGQDs@NC@Pd/GCE. (I) Quantitative cell viability results of CCK-8 assay. (J) Amperometric responses of NGQDs@NC@Pd/GCE to the addition of 0.1 mM fMLP and 500 U/mL catalase in tested well with U87 cells (a) and without cells (b). (K) Amperometric responses of NGQD@NC@Pd/GCE to the addition of 0.1 mM fMLP in tested well containing U87 cells without treatment (a), and two (b) and four (c) hours after the radiotherapy treatment. (L) Corresponding histograms of the amperometric responses of (K), using the U87 cells without treatment as control.

4. CONCLUSIONS

In summary, we have developed a high-performance electrochemical biosensor based on NGQD@NC@Pd HNSs by taking advantage of the synergistic effect derived from their unique structure and extraordinary electrocatalytic properties, and explored their clinical application in ultra-sensitive and highly specific detection of H_2O_2 secreted from living cancer cells. When implemented in an electrochemical sensing system, Pd NPs and NGQD incorporated in NC-HCSs architecture acted as dual signal-amplifying nanoprobes towards the target molecules, and NC-HNS materials served as a good support to facilitate the loading Pd NPs and NGQD upon it, and enhance their electrocatalytic activity and stability. Consequently, the non-enzymatic H_2O_2 biosensor based on NGQD@NC@Pd HNSs exhibited a collection of highly desirable sensing performances, including favorable operating potential, ultra-low detection limit, high sensitivity, reproducibility, stability, and anti-interference ability. For *in-vitro* detection of cancer, the proposed biosensing system demonstrated its ability to distinguish a trace amount of H_2O_2 released from various living cancer cells, as well as estimating the therapeutic effect of

chemotherapy and radiotherapy towards cancer. Thus, this study and its findings hold great promise for the pathological diagnosis and management of cancer diseases.

ASSOCIATED CONTENT

SEM image, TEM image, and XPS survey spectrum of NGQDs@NC@Pd HNSs. XPS survey spectra of NC@Pd composite. Scheme of the modification process of GCE. CV curves of NGQDs@NC@Pd/GCE, NGQDs@NC/GCE, and NC/GCE in 1.0 mM $K_3Fe(CN)_6$ +1.0 mM $K_4Fe(CN)_6$. CV curves of the amperometric response of NGQDs@NC/GCE and NC@Pd/GCE to successive addition of H_2O_2 in PBS buffer (pH 7.4). Amperometric response of eight different NGQD@NC@Pd/GCE to 20 μM H_2O_2. Table of sensing performances of several nonenzymatic H_2O_2 sensors based on different nanomaterials reported in the last year. Table of influence of foreign species on the determination of 50 μM H_2O_2. This material is available free of charge via the Internet at http://pubs.acs.org.

AUTHOR INFORMATION

Corresponding Author

*Address correspondence to chmsamuel@mail.hust.edu.cn (S. Wang); xiaofei@hust.edu.cn (F. Xiao).

Author Contributions

The manuscript was written through contributions of all authors. All authors have given approval to the final version of the manuscript. [§]These authors contributed equally.

Conflict of Interest: The authors declare no competing financial interest.

ACKNOWLEDGMENT

This research was financially supported by the National Natural Science Foundation of China (Project No. 51173055, No.51572094 and No. 21305048), and National Program on Key Basic Research Project (973 Program, Grant No. 2013CBA01600). We thank the Analytical and Testing Center of Huazhong University of Science and Technology and the Wuhan National Laboratory for Optoelectronics for AFM, SEM, TEM and XPS measurements.

REFERENCES

(1) Yang, H. W.; Lin, C. W.; Hua, M.Y.; Liao, S. S.; Chen, Y. T.; Chen, H. C.; Weng, W. H.; Chuang, C. K.; Pang, S. T.; Ma, C. C. M. Combined Detection of Cancer Cells and a Tumor Biomarker Using an Immunomagnetic Sensor For the Improvement of Prostate-Cancer Diagnosis. *Adv. Mater.* **2014**, 26, 3662–3666.

(2) Mishra, A.; Verma, M. Cancer Biomarkers: Are We Ready for the Prime Time?. *Cancers* **2010***, 2, 190–208.*

(3) Chikkaveeraiah, V.B.; Bhirde, A. A.; Morgan, N. Y.; Eden, H. S.; Chen, X. Y.; Electrochemical Immunosensors For Detection Of Cancer Protein Biomarkers. *ACS nano* **2012**, 6546-6561.

(4) Maji, S. K.; Sreejith, S.; Mandal, A. K.; Ma, X.; Zhao, Y. Immobilizing Gold Nanoparticles in Mesoporous Silica Covered Reduced Graphene Oxide: A Hybrid Material for Cancer Cell Detection Through Hydrogen Peroxide Sensing. *ACS Appl. Mater. Interfaces* **2014**, 6, 13648−13656.

(5) Halliwell, B.; Clement, M.V.; Ramalingam, J.; Long, L.H. Hydrogen Peroxide: Ubiquitous in Cell Culture and In Vivo? *IUBMB Life* **2000**, 50, 251–257.

(6) Hu, Y.; Rosen, D. G.; Zhou, Y.; Feng, L.; Yang, G.; Liu, J.; Huang, P. Mitochondrial Manganese-Superoxide Dismutase Expression in Ovarian Cancer Role in Cell Proliferation and Response to Oxidative Stress. *J. Biol. Chem.* **2005,** 280, 39485-39492.

(7) Sun, Y. M.; Zheng, H.; Wang, C.; Yang, M.; Zhou, A.; Duan, H. W. Ultrasonic-Electrodeposition of Ptpd Alloy Nanoparticles on Ionic Liquid-Functionalized Graphene Paper: Towards A Flexible And Versatile Nanohybrid Electrode. *Nanoscale* **2016**, *8*, 1523–1534.

(8) Gorodetskaya, I. A.; Gorodetsky, A. A. Analytical Chemistry: Clamping Down On Cancer Detection. *Nat. Chem.* **2015**, 7, 541–542.

(9) Xiang, Y.; Lu, Y. Using Personal Glucose Meters and Functional DNA Sensors to Quantify a Variety of Analytical Targets. *Nature Chem.* **2011**, 3, 697–703.

(10) Hsieh, K.; Patterson, A. S.; Ferguson, B.S.; Plaxco, K. W.; Soh, H. T. Rapid, Sensitive, And Quantitative Detection of Pathogenic DNA At The Point of Care Via Microfluidic Electrochemical Quantitative Loop-Mediated Isothermal Amplification (MEQ-LAMP). *Angew Chem. Int. Ed.* **2012**,*124,* 4980–4984.

(11) Kelley, S. O.; Mirkin, C. A.; Walt, D. R.; Ismagilov, R. F.; Toner, M.; Sargent, E. H. Advancing The Speed, Sensitivity and Accuracy of Biomolecular Detection Using Multi-Length-Scale Engineering. *Nat. Nanotechnol.* **2014**, *9,* 969–980.

(12) Yu, C.; Wang, L.; Li, W.; Zhu, C.; Bao, N.; Gu, H. Detection of Cellular H_2O_2 in Living Cells Based on Horseradish Peroxidase At The Interface of Au Nanoparticles Decorated Graphene Oxide. *Sensor Actuat B: Chem.***2015**, *211,* 17–24.

(13) Ansari, S. A.; Husain, Q. Potential Applications of Enzymes Immobilized On/In Nano Materials: A Review. *Biotechnol. Adv.* **2012**, *30,* 512–523.

(14) Jia, X. F.; Dong, S. J.; Wang, E. K. Engineering The Bioelectrochemical Interface Using Functional Nanomaterials and Microchip Technique toward Sensitive and Portable Electrochemical Biosensors. *Biosens Bioelectron.* **2016**, *76,* 80–90.

(15) Zhu, C. Z.; Yang, G. H.; Li, H.; Du, D.; Lin, Y. H. Electrochemical Sensors and Biosensors Based on Nanomaterials and Nanostructures. *Anal. Chem.* **2015**, *87,* 230–249.

(16) Zhu, H. Y.; Sigdel, A.; Zhang, S.; Su, D.; Xi, Z.; Li, Q.; Sun, S. H. Core/Shell Au/Mno Nanoparticles Prepared Through Controlled Oxidation Of Aumn As An Electrocatalyst for Sensitive H_2O_2 Detection. *Angew. Chem. Int. Ed.* **2014**, *53,* 12508–12512.

(17) Xiao, F.; Li, Y. Q.; Zan, X. L.; Liao, K.; Xu, R.; Duan, H. W. Growth Of Metal–Metal Oxide Nanostructures on Freestanding Graphene Paper for Flexible Biosensors. *Adv. Funct. Mater.* **2012**, *22,* 2487–2494.

(18) Xiao, F.; Song, J. B.; Gao, H.; Zan, X. L. Xu, R.; Duan, H. W. Coating Graphene Paper With 2D-Assembly Of Electrocatalytic Nanoparticles: A Modular Approach toward High-Performance Flexible Electrodes. *ACS Nano* **2012**, 6,100–110.

(19) Zhang, Z. H.; Zhang, R.; Li, C. C.; Yuan, L.; Li, P. P.; Yao, L.; Liu, S. Q. Nitrogen-Doped Carbon Hollow Spheres for Immobilization, Direct Electrochemistry, and Biosensing of Protein. *Electroanalysis* **2012,** *24*, 1424–1430.

(20) Jiang, D.; Du, X. J.; Liu, Q.; Hao, N.; Qian, J.; Dai, L. M.; Mao, H. P.; Wang, K. Anchoring AgBr Nanoparticles on Nitrogen-doped Graphene for Enhancement of Electrochemiluminescence and Radical Stability. *Chem. Commun.* **2015,** *51*, 4451–4454.

(21) Jiang, D.; Liu, Q.; Wang, K.; Qian, J.; Dong, X. Y.; Yang, Z. T.; Qiu, B. J. Enhanced Non-

enzymatic Glucose Sensing Based on Copper Nanoparticles Decorated Nitrogen-doped Graphene. *Biosens. Bioelectron.* **2014,** *54*, 273–278.

(22) Jiang, D.; Du, X.; Liu, Q.; Zhou, L.; Qian, J.; Wang, K. (2015). One-step Thermal-treatment Route to Fabricate Well-dispersed ZnO Nanocrystals on Nitrogen-doped Graphene for Enhanced Electrochemiluminescence and Ultrasensitive Detection of Pentachlorophenol. *ACS Appl. Mater. Interfaces* **2015,** *7,* 3093–3100.

(23) Xi, J. B.; Zhang, Y.; Wang, N.; Wang, L.; Zhang, Z. Y.; Xiao, F.; Wang, S. Ultrafine Pd Nanoparticles Encapsulated in Microporous Co_3O_4 Hollow Nanospheres for In Situ Molecular Detection of Living Cells. *ACS Appl. Mater. Interfaces* **2015**, *7,* 5583–5590.

(24) Han, M.; Liu, S. L.; Bao, J. C.; Dai, Z. H. Pd Nanoparticle Assemblies - As The Substitute Of HRP, In Their Biosensing Applications for H_2O_2 and Glucose. *Biosens. Bioelectron.* **2012**, *31,* 151–156.

(25) Dong, Y. Q.; Shao, J. W.; Chen, C. Q.; Li, H.; Wang, R. X.; Chi, Y. W.; Lin, X. M.; Chen, G. N. Blue Luminescent Graphene Quantum Dots And Graphene Oxide Prepared by Tuning the Carbonization Degree of Citric Acid. *Carbon* **2012**,*50,* 4738 –4743.

(26) Wei, H.; Wang, E. K. Nanomaterials With Enzyme-Like Characteristics (Nanozymes): Next-Generation Artificial Enzymes. *Chem. Soc. Rev.* **2013**, *42,* 6060–6093.

(27) Lin, L. P.; Song, X. H.; Chen, Y. Y.; Rong, M. C.; Zhao, T. T.; Wang, Y. R.; Jiang, Y. Q.; Chen, X. Intrinsic Peroxidase-Like Catalytic Activity of Nitrogen-Doped Graphene Quantum Dots and Their Application in The Colorimetric Detection of H_2O_2 and Glucose. *Anal. Chim. Acta* **2015**, *869,* 89–95.

(28) Wang, G.; Sun, Y. H.; Li, D. B.; Liang, H. W.; Dong, R. H.; Feng, X. L.; Müllen, K. Controlled Synthesis of N-Doped Carbon Nanospheres With Tailored Mesopores Through Self-Assembly of Colloidal Silica. *Angew. Chem. Int. Ed.* **2015**, *54,* 1–7.

(29) Chen, M.; Ye, C. Y.; Zhou, S. X.; Wu, L. M. Recent Advances in Applications and Performance of Inorganic Hollow Spheres in Devices. *Adv. Mater.* **2013**, *25,* 5343–5351.

(30) Lee, J. S.; You, K. H.; Park, C. B. Highly Photoactive, Low Bandgap TiO_2 Nanoparticles Wrapped by Graphene. *Adv. Mater.* **2012**, *24,* 1084–1088.

(31) Lee, H.; Dellatore, S. M.; Miller, W. M.; Messersmith, P. B. Mussel-Inspired Surface Chemistry for Multifunctional Coatings. *Science* **2007**, *318,* 426–430.

(32) Sun, T.; Zhang, Z. Y.; Xiao, J. W.; Chen, C.; Xiao, F.; Wang, S.; Liu, Y. Q. Facile And Green Synthesis Of Palladium nanoparticles-Graphene-Carbon Nanotube Material with High Catalytic Activity. *Sci. Rep.* **2013**, *3,* 2527.

(33) Zhu, Q.; Pan, Q. M. Mussel-Inspired Direct Immobilization of Nanoparticles and Application for Oil–Water Separation. *ACS nano* **2014**, *8,* 1402–1409.

(34) Gao, H. C.; Sun, Y. M.; Zhou, J. J.; Xu, R.; Duan, H. W. Mussel-Inspired Synthesis of Polydopamine-Functionalized Graphene Hydrogel as Reusable Adsorbents for Water Purification. *ACS Appl. Mater. Interfaces* **2013**, *5,* 425–432.

(35) Kong, X. K.; Sun, Z.; Chen, M.; Chen, Q. W. Metal-Free Catalytic Reduction of 4-Nitrophenol to 4-Aminophenol By N-Doped Graphene. *Energy Environ. Sci.* **2013**, *6,* 3260–3266.

(36) Pisarevskaya, E. Y.; Zolotarevskiy, V. I.; Kazanskiy, L. P.; Ovsyannikova, E. V.; Alpatova, N. M. Double-Stage Poly-O-Phenylenediamine Modification with Palladium Nanoparticles. *Synth. Met.* **2009**, *159,* 304–310.

(37) Zoski, C. G. Handbook of Electrochemistry (1st ed), Elsevier, Amsterdam, **2007**.

(38) Sun, Y. M.; He, K.; Zhang, Z. F.; Zhou, A. J.; Duan, H. W. Real-Time Electrochemical Detection of Hydrogen Peroxide Secretion in Live Cells by Pt Nanoparticles Decorated Graphene-Carbon Nanotube Hybrid Paper Electrode. *Biosens. Bioelectron.* **2015**, *68,* 358–364.

(39) Liu, J.; Bo, X. J.; Zhao, Z.; Guo, L. P. Highly Exposed Pt Nanoparticles Supported on Porous Graphene For Electrochemical Detection of Hydrogen Peroxide in Living Cells. *Biosens. Bioelectron.* **2015**, *74,* 71–77.

(40) Wang, L.; Zhang, Y. Y.; Cheng, C. S.; Liu, X. L.; Jiang, H.; Wang, X. M. Highly Sensitive Electrochemical Biosensor for Evaluation of Oxidative Stress Based on the Nanointerface of Grapheme Nanocomposites Blended with Gold, Fe_3O_4, and Platinum Nanoparticles. *ACS Appl. Mater. Interfaces* **2015**, *7,* 18441–18449.

(41) Xiao, C.; Liu, Y. L.; Xu, J. Q.; Lv, S. W.; Guo, S.; Huang, W. H. Real-Time Monitoring of H_2O_2 Release From Single Cells Using Nanoporous Gold Microelectrodes Decorated with Platinum Nanoparticles. *Analyst* **2015**, *140,* 3753–3758.

(42) Cheng, C. M.; Huang, Y.; Wang, N.; Jiang, T.; Hu, S.; Zheng, B. Z.; Yuan, H. Y.; Xiao, D. Facile Fabrication of Mn_2O_3 Nanoparticle-Assembled Hierarchical Hollow Spheres and Their Sensing for Hydrogen Peroxide. *ACS Appl. Mater. Interfaces* **2015**, *7,* 9526–9533.

(43) Han, L.; Yang, D. P.; Liu, A. H. Leaf-Templated Synthesis of 3D Hierarchical Porous Cobalt Oxide Nanostructure As Direct Electrochemical Biosensing Interface with Enhanced Electrocatalysis. *Biosens. Bioelectron.* **2015**, *63,* 145–152.

(44) Kong, L. J.; Ren, Z. Y.; Zheng, N. N.; Du, S. C.; Wu, J.; Tang, J. L.; Fu, H. G. Interconnected 1D Co_3O_4 Nanowires On Reduced Graphene Oxide for Enzymeless H_2O_2 Detection. *Nano Res.* **2015**, *8,* 469–480.

(45) Ma, M.; Miao, Z. Y.; Zhang, D.; Du, X.; Zhang, Y. Y. Zhang, C.; Lin, J. H. Chen, Q. Highly-Ordered Perpendicularly Immobilized FWCNTs on The Thionine Monolayer-Modified Electrode for Hydrogen Peroxide And Glucose Sensors. *Biosens. Bioelectron.* **2015**, *64,* 477–484.

(46) Yang, J.; Zhou, B.; Yao, J.; Jiang, X. Q. Nanorods of A New Metal–Biomolecule Coordination Polymer Showing Novel Bidirectional Electrocatalytic Activity and Excellent Performance in Electrochemical Sensing. *Biosens. Bioelectron.* **2015**, *67*, 66–72.

(47) Hao, C.; Shen,Y. R.; Wang, Z. Y.; Wang, X. H.; Feng, F.; Ge, C. G.; Zhao, Y. T.; Wang, K. Preparation and Characterization of Fe_2O_3 Nanoparticles by Solid-Phase Method and Its Hydrogen Peroxide Sensing Properties. *ACS Sustainable Chem. Eng.* DOI: 10.1021/acssuschemeng.5b01150.

(48) World Health Organization. World Cancer Report. 2014, *WHO Report. Geneva: WHO,* **2014**, Chapter 1.1.

(49) Ma, R.; Zhang, D.; Hu, P. C.; Li, Q.; Lin, C. Y. HOXB7-S3 Inhibits The Proliferation and Invasion of MCF-7 Human Breast Cancer Cells. *Mol. Med. Rep.* **2015**, *12,* 4901–4908.

(50) Panaro, M. A.; Mitolo, V. Cellular Responses to FMLP Challenging: A Mini-Review. *Immunopharmacol. Immunotoxicol.* **1999**, *21,* 397–419.

(51) Yu, C. M.; Wang, L.; Li, W. B.; Zhu, C.; Bao, N.; Gu, H. Y. Detection Of Cellular H_2O_2 in Living Cells Based on Horseradish Peroxidase at the Interface of Au Nanoparticles Decorated Graphene Oxide. *Sens. Actuators, B* **2015**, *211*, 17–24.

(52) Bienert, G. P.; Schjoerring, J. K.; Jahn, T. P. Membrane Transport of Hydrogen Peroxide. *Biochim. Biophys.Acta, Biomembr.* **2006**, *1758,* 994–1003.

(53) Bienert, G. P.; Møller, A. L.; Kristiansen, K. A.; Schulz, A.; Møller, I. M.; Schjoerring, J. K.; Jahn, T. P. Specific Aquaporins Facilitate the Diffusion of Hydrogen Peroxide Across Membranes. *J. Biol. Chem.* **2007**, *282,* 1183–1192.

(54) Lippard S. J. (Ed.), *ACS Symposium Series 209, American Chemical Society,* Washington, D. C., **1983**.

(55) Sherman, S.; Lippard, S. J. Structural Aspects of Platinum Anticancer Drug Interactions with DNA. *Chem. Rev.* **1987**, *87,* 1153–1181.

(56) Ye, M. X.; Zhao, Y. L.; Li, Y.; Miao, Q.; Li, Z. K.; Ren, X. L.; Song, L. Q.; Yin, H.; Zhang, J. Curcumin Reverses Cis-Platin Resistance and Promotes Human Lung Adenocarcinoma A549/DDP Cell Apoptosis Through HIF-1α And Caspase-3 Mechanisms. *Phytomedicine* **2012**, *19,* 779–787.

(57) Wang, J.; Li, Q.; Chen, B.; Jiang, H. Layer-By-Layer Assembly of Graphene, Au and Poly(Toluidine Blue O) Films Sensor for Evaluation of Oxidative Stress of Tumor Cells Elicited by Hydrogen Peroxide. *Biosens. Bioelectron.* **2013**, *41,* 789–794

(58) Carro, M. S. Lim, W. K.; Alvarez, M. J.; Bollo, R. J.; Zhao, X.; Snyder, E. Y.; Sulman, E. P.; Anne, S. L.; Doetsch, F.; Colman, H.; Lasorella, A.; Aldape, K.; Califano, A.; Iavarone, A. Transcriptional Network for Mesenchymal Transformation Of Brain Tumours. *Nature* **2010**, *463,* 318–325.

(59) Jürchott, K.; Guo, K. T.; Catchpole, G.; Feher, K.; Willmitzer, L.; Schichor, C.; Selbig, J. Comparison Of Metabolite Profiles in U87 Glioma Cells and Mesenchymal Stem Cells. *Biosystems* **2011**, *105,* 130–139.

(60) Wachsberger, P. R.; Burd, R.; Cardi, C.; Thakur, M.; Daskalakis, C.; Holash, J.; Yancopoulos, G. D.; Dicker, A. P. VEGF Trap in Combination with Radiotherapy Improves Tumor Control in U87 Glioblastoma. *Int. J. Radiat.Oncol. Biol. Phys.* **2007**, *67,* 1526–1537.

(61) Gorrini, C.; Harris, I. S.; Mak, T. W. Modulation of Oxidative Stress as an Anticancer Strategy. *Nat. Rev. Drug Discovery* **2013**, *12,* 931–947.

(62) Ma, W. B.; Li, C. Y.; Yin, S. K.; Liu, J. X.; Gao, C.; Lin, Z. X.; Huang, R. Q.; Huang, J. F.; Li, Z. Y. Novel Role of TRPV2 in Promoting The Cytotoxicity of H_2O_2-Mediated Oxidative Stress in Human Hepatoma Cells. *Free Radical Bio. Med.* **2015**, *89*, 1003–1013.

Table of Contents Graphic